

Local properties of patterned vegetation: quantifying endogenous and exogenous effects

Gopal G. Penny^{1,*}, Karen E. Daniels², Sally E. Thompson¹

[1] Department of Civil and Environmental Engineering, University of California, Berkeley, California, 94710, sally.thompson@berkeley.edu

[2] Department of Physics, North Carolina State University, Raleigh, NC 27695, kdaniel@ncsu.edu

***Corresponding author:** Gopal G. Penny
Department of Civil and Environmental Engineering,
University of California,
Berkeley, California, 94710
Email: gopal@berkeley.edu
Phone: (+1) 510 642 1980
Fax: (+1) 510 643 5264

Running title: Local properties of patterned vegetation

Keywords: arid ecosystems; pattern formation

Manuscript type: submitted to Special Issue on “Pattern Formation in the Geosciences”

Abstract

Dryland ecosystems commonly exhibit periodic bands of vegetation, thought to form due to competition between individual plants for heterogeneously distributed water. In this paper, we develop a Fourier method for locally identifying the pattern wavenumber and orientation, and apply it to aerial images from a region of vegetation patterning near Fort Stockton, Texas. We find that the local pattern wavelength and orientation are typically coherent, but exhibit both rapid and gradual variation driven by changes in hillslope gradient and orientation, the potential for water accumulation, or soil type. Endogenous pattern dynamics, when simulated for spatially homogeneous topographic and vegetation conditions, predict pattern properties that are much less variable than the orientation and wavelength observed in natural systems. Our local pattern analysis, combined with ancillary datasets describing soil and topographic variation, highlights a largely unexplored correlation between soil depth, pattern coherence, vegetation cover and pattern wavelength. It also, surprisingly, suggests that downslope accumulation of water may play a role in changing vegetation pattern properties.

1. Introduction

Pattern formation occurs in numerous ecological and biological systems, where it has been linked to reaction-diffusion (Turing) type instabilities (Rietkerk *et al.*, 2002), hydrodynamic instabilities (Thompson & Daniels, 2010), and potential
5 (variational) dynamics that maximize or at least increase ecological productivity (Lefever *et al.*, 2009; Pringle *et al.*, 2010). Patterns have been observed in dryland vegetation (Borgogno *et al.*, 2009), in bogs and wetlands (Rietkerk *et al.*, 2004b; Larsen & Harvey, 2011), in mussel beds (Van de Koppel *et al.*, 2008), termite mounds (Pringle *et al.*, 2010) and other systems (Rietkerk *et al.*, 2004a).
10 In many cases ecological patterns form an intermediate realization between environmental states in which the entire landscape is either colonized or bare. As such they often indicate the presence of bistable states, which are characterized by the potential for critical and locally irreversible transitions (Scheffer *et al.*, 2009). Observations and theoretical work both suggest that transitions between
15 vegetated and desertified (unvegetated) conditions in patterned systems are preceded by striking changes in the morphology of the vegetation patterns, which thus act as an early-warning sign of deteriorating ecosystem health (Kefi *et al.*, 2007). Understanding the controls on the morphology of vegetation patterns therefore has practical interest in terms of ensuring that observed changes are
20 interpreted correctly.

Vegetation pattern formation in dryland ecosystems is a global phenomenon, ranging from random distributions of bare soil and vegetation canopies (Caylor *et al.*, 2004) to highly organized spatial distributions with identifiable length-scales and orientations (HilleRisLambers *et al.*, 2001; Rietkerk *et al.*, 2002;
25 Borgogno *et al.*, 2009). Intermediate cases such as power-law (scale-free) clustering (Scholes & Archer, 1997; Scanlon *et al.*, 2007; von Hardenberg *et al.*, 2010), and dendritic structures in which vegetation concentrates along drainage lines (McGrath *et al.*, 2012; Thompson *et al.*, 2011a) are also observed. All of these morphologies can be related to the presence, strength and directionality of
30 positive feedbacks that concentrate resources (such as nutrients, soil carbon and water) that sustain plant life in a localized region near the plants (Ravi *et al.*, 2008; Greene, 1992; Galle *et al.*, 1999; Harman *et al.*, 2012; Puigdefábregas, 2005; Schlesinger *et al.*, 1990). These feedbacks have lead to the moniker ‘ecosystem engineers’ being applied to perennial plants in dryland ecosystems:
35 they create the conditions necessary for their own survival (Gilad *et al.*, 2004; Yizhaq *et al.*, 2005).

The formation of periodic vegetation patterns is strongly linked to the coupling of (i) water redistribution to the vicinity of plants, and (ii) competition
40 between individual plants for access to this water resource (Borgogno *et al.*, 2009; Bromley *et al.*, 1997; Lefever *et al.*, 2009; Seghieri *et al.*, 1997). The dynamics of patterned vegetation systems has formed a focus of ecohydrological and nonlinear dynamics research, motivated by the increasingly well-demonstrated connection between pattern morphology and desertification

risk (Rietkerk *et al.*, 2002; Kefi *et al.*, 2007; Barbier *et al.*, 2008; Deblauwe
45 *et al.*, 2011); and by the inherently interesting nonlinear dynamics of these
systems (Lefever *et al.*, 2009; Meron *et al.*, 2004). Field and theoretical work
has identified the important roles of vegetation dynamics (Kefi *et al.*, 2007),
seed dispersal processes (Thompson *et al.*, 2008; Thompson & Katul, 2009), root
morphology (Barbier *et al.*, 2008; Lefever *et al.*, 2009), surface flow dynamics
50 (Thompson *et al.*, 2011b) and climate feedbacks (Konings *et al.*, 2011) in
modulating pattern morphology.

While our understanding of vegetation pattern dynamics is improving, there
remain undeniable differences between simulated vegetation patterns and the
natural ones observed in the field. Natural patterns are characterized by a
55 degree of disorder and heterogeneity on multiple scales that is not reproduced
in idealized models. Disorder can arise intrinsically through the existence of a
range of stable wavelengths and orientations, with transitions in space and time
occurring through local pattern pattern defects (Cross & Hohenberg, 1993). In
addition, the pattern wavelength and orientation can be strongly influenced by
60 either wavelength-scale inhomogeneities (Lowe *et al.*, 1983) or larger gradients
(Eckhaus & Kuske, 1997) in the underlying system, as well as the presence of
boundaries (Hu *et al.*, 1993) or noise (Lindner, 2004).

In natural systems, this means that disorder observed in vegetation patterns
could either reflect intrinsic features of the pattern forming process (*endogenous*
65 *effects*), or could reflect spatial changes in soil structure and local topography
(*exogenous effects*). For instance, Thompson *et al.* (2008) explored whether the
unrealistically smooth nature of many models of vegetation biomass distribution
was an artifact of representing seed dispersal as a diffusive process. Greater
fidelity between modeled and observed (disordered) vegetation patterns was
70 achieved by representing plant population migration with a seed dispersal kernel.
More simply, theoretical treatments of vegetation patterning usually neglect
variations in soils and topography, or impose periodic boundary-conditions that
remove the differences in water availability between the top and bottom of a
hillslope. Such simplifications will inevitably lead to idealized representations
75 of the vegetation response and obscure interactions between the intrinsic pattern
structure and the spatial structure of the landscape. For example, McGrath
et al. (2012) demonstrated that the orientation and wavelength of vegetation
patterns modeled with realistic boundary conditions changed between the top and
bottom of the hillslope. In control simulations with periodic boundary conditions,
80 vegetation bands formed with a single wavelength and were orientated at 90° to
the direction of water flow, in agreement with other modeling studies. When
realistic boundary conditions were imposed, however, the bands near the top of
the hillslope curved to lie perpendicular to the ridgeline. Similarly, the effects
of spatial heterogeneity in soil properties on pattern formation have not been
85 widely explored (although see Thompson *et al.* (2008)). A number of theoretical
studies indicate that local biomass, band properties and band coherence should
vary with changing minimum and maximum infiltration capacities and soil

properties (Ursino & Contarini, 2006; Thiéry *et al.*, 1995), and there are some tantalizing hints that subsurface features, such as the ironstone underlying tiger
90 bush in Niger, calcrete hardpans underlying banded patterns in Texas, and
silcrete hardpans underlying *mulga* bands in Australia (McDonald *et al.*, 2008;
White, 1970; Mabbutt & Fanning, 1987), may have an association with patterned
vegetation.

Predictions about the interaction of vegetation patterns with changing soil
95 or topography can be investigated using remotely sensed datasets, an approach
with a long and growing history. Vegetation patterns in Africa were first
observed from light aircraft flights (Macfadyen, 1950; Worrall, 1960). Initial
analyses of the patterns demonstrated their spatial regularity on the basis of the
two-dimensional Fourier power spectrum (Couteron & Lejeune, 2001). More
100 recently, Deblauwe *et al.* (2011) undertook large scale analyses of morphological
trends in vegetation patterns in the Sudan by linking several remotely sensed
datasets: surface imagery from the System for Earth Observation (SPOT)
satellite, topographic data from the Shuttle Radar Topography Mission (STRM),
and rainfall data from the Tropical Rainfall Measuring Mission (TRMM). This
105 allowed analysis of pattern morphology at 400 m resolution over multiple square
kilometers. Although higher resolution datasets are available, they have generally
either been analyzed only over relatively small spatial scales ($\approx 1 \text{ km}^2$) (Barbier
et al., 2008) or investigated from the perspective of identifying morphological
change over time (Deblauwe *et al.*, 2012).

110 A key open question is therefore to characterize small-scale irregularities
in vegetation patterns, and to classify them based on whether they arise due to
either endogenous dynamics or variation in exogenous features imposed by the
landscape. Understanding the implications of such variation on the resilience
and stability of the ecosystems has important consequences for identifying and
115 preventing potential desertification.

In this paper, we report on the development of methods suitable for
quantifying local patterns within high-resolution aerial photography, and for
relating those features to ancillary datasets describing soil and topographic
variation. Our site, located near Fort Stockton, Texas (see McDonald *et al.*
120 (2008)) was selected because it exhibits vegetation bands and also offers several
characteristics that facilitate studies of covariation. First, the aerial photography
covers a large region at a resolution (0.5 and 1 m) comparable to the diameter
of perennial vegetation canopies, allowing for the observation of individual
plants. Second, high resolution (10 m spatial, 15 cm vertical) elevation datasets
125 are available from the US National Elevation Dataset, allowing changes in the
orientation and gradient of the hillslope to be mapped on scales that are much
less than the pattern wavelength. Finally, the study area has been mapped as
part of the SSURGO national soils database, and contains considerable variation
in soil type. The availability of these datasets provides a valuable opportunity
130 to investigate correlations between vegetation patterning and soil characteristics
over tens of square kilometers.

Our analysis depends on these spatial datasets, and is subject to their inherent limitations. These limitations include the resolution, spatial artifacts, and the risk of spurious correlation, given that vegetation features are often considered when mapping soil boundaries. To minimize the effects of issues, we focus on two large-scale hypotheses: (1) The wavelength and orientation of the vegetation pattern are locally coherent but exhibit both rapid and gradual variation; and (2) The variability in vegetation pattern features will correlate with soil and elevation features in predictable ways. We note that by focusing on soil and topographic features, we inherently assume that spatial variations in pattern morphology arise due to spatial heterogeneity in landscape properties, rather than due to the nonlinear dynamics of the pattern forming process itself. In patterns far from threshold, features such as defects, dislocations, grain boundaries, and boundary conditions can result in spatial heterogeneity in pattern properties, *even* when all other fields are homogeneous (Cross & Greenside, 2009). To control for this possibility, we also briefly address the following null hypothesis: (3) Large-scale variations in pattern properties can be explained by the nonlinear interactions associated with vegetation pattern formation.

We test the major hypotheses through the development of a localized Fourier technique to identify pattern wavenumber and direction. To address Hypothesis 1, this technique was applied to high (0.5 m) resolution aerial photography. To address Hypothesis 2, the technique was applied to a 188 km² area, allowing local pattern properties to be correlated to the site soil and topographic properties. Hypothesis 3 was tested by identifying a subset of the 0.5 m resolution image containing banded patterns that were close to ideal (i.e. reproducible by a model). We applied the Fourier analysis technique to both observed and simulated patterns, and compared variability in the wavenumber and direction fields in the modeled and observed patterns.

We find that our two major hypotheses are satisfied. Local patterns are oriented in the same direction as the topographic slope and the pattern wavelength decreases for steeper gradients. Deviations from these trends are associated with the presence of ridges, stream channels, anthropogenic features or changes in soil type. Different soil types within the study area determine the pattern boundaries and the pattern morphology: shallow soils are associated with highly coherent, shorter wavelength patterns, and deep soils with patterns that become incoherent and increase in wavelength near stream channels. Finally, the modeling test validated our decision to focus on landscape and soil features. Even in the most uniform region of the observed patterns, the variability in the real pattern properties exceeded that which could be retained in the steady state solution of a physical model that closely reproduced the mean pattern properties.

2. Methods

(a) Study Site and Data

The study site is a 188 km² area located approximately 30 km NW of Fort Stockton, Texas (coordinates: 31°05' N, 103°03' W) (National Climatic Data Center, 2010). The climate is hot and dry, receiving 370 mm annual rainfall on average, mean summer maximum temperatures of approximately 35°C and winter minima near freezing. The site is part of a large cattle ranch and is used for grazing. Dominant vegetation species include tarbush (*Flourensia cenea*), bunch and sod grasses (*Aristida purpurea*, *Bouteloua curtipendula* and *Scleropogon brevifolius*), and mixed mesquite (*Prosopis glandulosa*) and juniper (*Juniperus pinchotti*) brush (McDonald *et al.*, 2008). The site contains a striking spatial pattern consisting of bands of continuous vegetation cover lying over bare soil (McDonald *et al.*, 2008); see Fig. 1.

High resolution imagery (0.5 m and 1 m pixels) were obtained from Digital Globe, and from the National Agricultural Imaging Project (National Agricultural Imaging Program, 2010). We used the highest resolution images from Digital Globe for fine-scale analysis and a comparison between modeled and observed pattern morphology. We analyzed the NAIP images, which cover the whole area, to relate local pattern properties to soil and topographic features.

We classified the image pixels as 'vegetation' or 'no vegetation' using a supervised classification based on total brightness (Richards, 1999). We used brightness because the perennial vegetation was not actively photosynthesizing when the photographs were taken, meaning that standard vegetation indices could not discriminate the vegetated locations. An example of the resulting binary image is shown in Fig. 1. Darker colors represent vegetation cover and the lighter colors bare soil. The insets show an original and classified image over a 260 × 260 m² window.

(b) Fourier Windowing Method

To quantitatively test our hypotheses, we developed a quasi-local technique to measure pattern wavelength λ and pattern orientation Θ for the binary images. The technique provides information about the local wavevector $\vec{k} = k_x\hat{x} + k_y\hat{y}$, similar to that provided by short-time Fourier transforms or wavelet based approaches used in timeseries analysis (Allen & Rabiner, 1977; Daubechies, 1990). Local wavevectors are useful for classifying convection patterns (Heutmaker *et al.*, 1985) and for identifying pattern defects (Egolf, 1998; Daniels *et al.*, 2008). Here we applied a two-dimensional Fourier transform to obtain the power spectrum within a square, moving window. Local wavelength and pattern orientation were identified for each window, and the results averaged for all windows that spanned a given location. This straightforward technique is suitable for identifying the dominant pattern properties in noisy images with irregular patterning. More elegant and rigorously-local techniques, based on the

ratios of the spatial derivative of the banding pattern (Egolf, 1998), could not be applied because the vegetation bands deviate substantially from a sinusoidal pattern in space. The drawbacks of the short-time Fourier transform—namely the
215 tendency to truncate long wavelengths due to the finite window size, and poor localization of short-wavelength components (Pinnegar & Mansinha, 2004)—do not pose significant difficulties in the current application, provided that the window size is greater than the local wavelength of the pattern.

For each window of size $L \times L$, we obtained the 2D fast Fourier transform
220 $\tilde{f}(k_x, k_y)$ of the pattern $f(x, y)$. For each window's $\tilde{f}(\vec{k})$, we calculated the power spectrum $S(\vec{k}) = |\tilde{f}(\vec{k})|^2$. As L increases, the likelihood of identifying a single wavelength and orientation decreases. Conversely, as L decreases, the k -resolution in Fourier space is reduced. To optimize both the localization of measurements and the resolution, we chose L to be at least 5λ . The window was
225 applied to overlapping regions of the pattern at 20 m intervals.

The power spectrum measures the power contributed to the pattern by each wavevector \vec{k} . To separate the local wavelength from its orientation, we decomposed each \vec{k} into its magnitude (wavenumber) $k = \sqrt{k_x^2 + k_y^2} = 2\pi/\lambda$ and its orientation θ . Due to symmetry, the pattern orientation can be defined only
230 between 0 and π . To identify the dominant k in each window, we binned $S(\vec{k})$ into annular rings of width $k = 6\pi/L$. To deconvolve the natural $1/k$ scaling of the image (Burton & Moorhead, 1987; Tolhurst *et al.*, 1992), we computed the total power within each annular ring, $S(k)$. The location peak of this total power (rather than the mean power) is used to define the most energetic wavenumber,
235 k_1 . To compensate for the large bin width, we computed the location of the weighted average $k_1 \equiv \langle kS(k) \rangle / \langle S(k) \rangle$ over all rings that formed part of the peak and contained $> 75\%$ of the peak power. We discarded windows where k_1 corresponded to the limits of the window function or pixel resolution, and, to avoid discarding sites where L truncated λ , visually confirmed that these
240 windows corresponded to un-patterned areas. Finally, we discarded windows where the mean power of the pattern-forming wavenumber was less than that of noise. To determine the dominant pattern orientation, we binned $S(\vec{k})$ into segments of width $\pi/8$ and computed the average power, $S(\theta)$. The dominant orientation was located via the weighted average $\theta_1 \equiv \langle \theta S(\theta) \rangle / \langle S(\theta) \rangle$. The most energetic values (k_1, θ_1) for each window were used to generate spatial maps
245 $\lambda(x, y)$ and $\Theta(x, y)$ representing the local pattern wavelength and orientation. For each x, y location, the assigned value of λ and Θ comes from the average $2\pi/k$ and θ of all windows which include that x, y .

Although the procedure so far assumes a two-dimensional pattern with a single wavelength and orientation within each window, the power spectra regularly contained additional peaks. We evaluated the uniqueness of the local pattern properties by comparing the dominant peak to its most distant energetic peak. Energetic peaks were defined as those containing $> 75\%$ of the power of the dominant peak. The most distant peak was then defined as the energetic

peak with wavenumber k_2 and orientation θ_2 that maximized $|k_1 - k_2|$ and $|\theta_1 - \theta_2|$. Uniqueness metrics were then defined for both the wavenumber and the orientation as:

$$Q_k = 1 - \frac{|k_1 - k_2|}{\max(k_1, k_2)} \quad (2.1)$$

$$Q_\theta = 1 - \frac{|\theta_1 - \theta_2|}{\pi/2}$$

Q_k and Q_θ quantify the degree to which the dominant peak is either a unique energetic peak ($k_1 = k_2$ and $\theta_1 = \theta_2$ implies $Q_k = 1$ and $Q_\theta = 1$) or is one of at least 2 energetic peaks lying orthogonal to each other ($Q_\theta = 0$) or separated by a large relative distance in k space.

Matlab code that performs the Fourier Windowing Method outlined in this section is provided as online supplementary material.

(c) Construction of the spatial fields used for analysis

The local Fourier analysis was run twice, using windows with $L = 260$ m and $L = 400$ m, applying the window to overlapping regions on 20 m intervals, and generating smoothly-varying maps of the local pattern properties. The two window sizes ensured that the largest wavelengths could be analyzed ($L = 400$ m), and exploited the greatest feasible localization given the median pattern wavelengths ($L = 260$ m). The $L = 400$ m method identified large λ in regions where the $L = 260$ m method identified no pattern; while the $L = 260$ m method allowed the pattern properties to be identified in regions with dimensions < 400 m. To combine the outcome, we averaged the results of the analyses for overlapping cells (resulting in a minimum change in the identified Θ and λ), and retained the uniquely identified Θ and λ in cells where either mechanism failed. Since the pattern properties in windows located near the edges of the pattern are influenced by both patterned and unpatterned regions, we trimmed the resulting $\lambda(x, y)$ and $\Theta(x, y)$ fields by 130 m to discard the most strongly-affected regions. The results of the complete analysis are shown in Fig. 2.

We developed a map of the soil type on the 20 m grid by interpolating the SSURGO data. We smoothed the NED elevation data to remove high-resolution artifacts (Oimoen, 2000), and computed the topographic gradient (steepness) and aspect (orientation) over the same 20 m grid. We made direct comparisons between $\lambda(x, y)$, $\Theta(x, y)$ and the soil and topographic features. To cope with the large, noisy dataset, we grouped the data into bins of equal size and related the median and interquartile range of the local pattern characteristics to the predictor variables across the bins. The behavior of these summary statistics and the dataset was analyzed using least squares regression. We analyzed the frequency of occurrence of deviations between the pattern and hillslope orientations $\Delta\Theta$ and the frequency of occurrence of non-unique pattern orientation and wavelength Q_λ and Q_Θ as a function of location (e.g. near topographic minima (drainage

lines), maxima (ridges), anthropogenic features (roads and trails), and the edges of the pattern).

285 (d) *Comparison to models*

To quantify the degree to which local pattern variations can be explained as non-ideal pattern features that can arise from the nonlinear dynamics of the pattern forming mechanisms, we performed a control analysis using simulated data. Our test region is a $500 \times 800 \text{ m}^2$ region of the 0.5 m resolution pattern. Analyzed at the $200 \times 200 \text{ m}^2$ scale, the pattern in this region contained a single high-energy wavenumber and direction peak, indicating that it could be reasonably modeled with homogeneous model parameters. We used the pattern in this region as the initial condition for a physically-based vegetation band-forming model (Rietkerk *et al.*, 2002; Thompson & Katul, 2009). We used this model because it (a) represents the surface runoff feedback mechanisms that were observed to occur at this site by McDonald *et al.* (2008); and (b) simulates vegetation bands that retain curvature, variability and other non-ideal behaviors (compared to more idealized models (Lefever & Lejeune, 1997)) and thus has the potential to generate spatially variable pattern properties endogenously. We selected model parameters by stepping through reasonable parameter combinations and selecting the combination that minimized the variation between the observed vegetation pattern and the model prediction after 5000 timesteps (Thompson *et al.*, 2008). This method allows us to identify a parameter set for the model that approximates the observed patterns as a stable steady state solution. Using both the model output and the original binary images, we apply the same Fourier windowing method and compute key spatial statistics (mean, variance, and autocorrelation length, taken as the lag at which the autocorrelation halved) for the resulting $\lambda(x,y)$ and $\Theta(x,y)$.

3. Results

310 (a) *Local properties of vegetation patterns*

Using the Fourier windowing method, we find that 44% of the 188 km^2 area contains patterned vegetation with a clearly identifiable wavelength and orientation. The Fourier windowing method fails to detect some areas where vegetation patterns are visually identifiable. These include regions where vegetation bands are confined to fingers of a particular soil type that are $\lesssim 260 \text{ m}$ in extent, meaning that the pattern cannot be identified as the dominant Fourier mode in any given window. There are also some regions where a pattern can be identified by eye, but is so disordered that it falls below the noise threshold. Approximately 10% of the study area consists of isolated patches of patterning which offer little opportunity to explore spatial variations. Instead, we confine

our analysis to the 34% ($\approx 64 \text{ km}^2$) of the image that consists of spatially-connected vegetation patterns. Within these regions, the pattern has a mean wavelength of $\bar{\lambda} = 63 \pm 14 \text{ m}$ (reported variations are standard deviation unless otherwise specified) and an autocorrelation length of approximately 800 m (i.e. $\approx 12\bar{\lambda}$). The probability distribution function (PDF) of $\Theta(x,y)$ values is peaked in the north-south direction, but spans a full $0 \leq \Theta < \pi$ range. Table 1 provides summary statistics describing the average pattern characteristics, topography and soil properties.

While seven distinct soil types occur in the study area, two of these, the Delnorte and Reakor associations, contain 97% of the vegetation patterning. These soils are distinguished by a relatively low clay and high silt content. The Delnorte association is characterized by a very shallow soil depth (23 cm) due to the presence of calcium-carbonate based hardpan or petrocalcic horizon. By contrast, Reakor association soils are at least 2 m deep. The full range of soil properties is shown in Table 2.

We find that three factors broadly determine the local pattern properties: the orientation of the slope, the steepness of the slope, and the soil type. The orientation Θ of the pattern is almost completely determined by the underlying slope orientation. As illustrated in Fig. 3a, approximately 81% of the pattern is oriented within $\pm\pi/8$ radians of the hillslope. Deviations between the pattern and hillslope orientations, denoted $\Delta\Theta$, are discussed further in §3.c. Second, we observe a significant relationship between the local pattern wavelength λ and the hillslope gradient. Fig. 3b illustrates the moderately strong, significant decline in the median wavelength λ of equally sized data bins with increasing hillslope gradient ($r^2 = 0.63, p = 6 \times 10^{-3}$). In addition, we found that the pattern wavelength is influenced by the soil type. Fig. 3c shows PDFs of λ for each soil type. While Delnorte soils have a unimodal PDF (mode $\lambda = 53 \text{ m}$), the Reakor association soils have a bimodal distribution. One mode corresponds to that of the Delnorte soils ($\lambda = 52 \text{ m}$), but the other modal wavelength is much longer, with $\lambda = 71 \text{ m}$. Further analysis of this effect is provided in §3.d

(b) Comparison to models

The results are shown in Table 3. We find that while the mean properties of the model and observed pattern are similar (a consequence of calibrating the model to these means), Θ and λ vary 3 – 5 times more in the observed pattern than in the modeled pattern. The underlying topography is still more variable, and presumably causes the variability of the observed pattern. Thus, even in the region of the study site with the greatest uniformity in the pattern properties, the spatial heterogeneity observed in the real patterns exceeded the pattern variability that could be produced by a physical model. These results justify our attribution of the remaining variability in the pattern properties across the site to environmental variation rather than to defects or initial condition effects arising from the nonlinear dynamics of the system.

(c) *Non-uniqueness in pattern attributes*

365 While the local pattern wavelength and orientation is on average set by the
local hillslope gradient and orientation, we nonetheless observe regions with
significant deviation from the overall trend. As shown in Fig. 3a, the deviation
between pattern and hillslope orientation, $\Delta\Theta$, is $> \pi/8$ over approximately 20%
of the pattern. There are even regions in which $\Delta\Theta \approx \pi/2$, where the vegetated
bands run parallel rather than perpendicular to the local hillslope gradient. Fig. 4
370 shows the spatial distribution of the orientation uniqueness metric Q_θ across
the patterned region, highlighting regions of non-uniqueness. About half of the
windows with large $\Delta\Theta$ also contain more than one pattern direction (non-
uniqueness in $\Theta(x,y)$). As illustrated by Fig. 5, non-unique pattern orientations
are clustered near streams (50% increase in frequency of $Q_\theta < 0.75$ relative to
375 the remainder of the pattern), ridges (50% increase in frequency), roads (30%
increase in frequency), and the pattern edge. We also observe regions with large
deviations ($\Delta\Theta > \pi/8$) but nonetheless unique pattern orientations ($Q_\theta \geq 0.75$).
Such regions also occur near ridges and streams more frequently than in the
remainder of the pattern ($\approx 30\%$ more frequent in each case).

380 The insets in Fig. 4 illustrate regions of complexity in $\Theta(x,y)$. Fig. 4a and
Fig. 4b show regions of non-unique pattern directions. In Fig. 4a, we show a
perturbation of the local pattern by a road. As illustrated, the upslope edge
of roads is globally associated with increased vegetation, while the downslope
edges are typically bare. Roads thus generate linear features that can create
385 non-uniqueness in the local pattern orientation. This panel also shows a second
anthropogenic feature, a storm drainage outlet, which further decreases Q_θ west
of the road. Fig. 4b illustrates how changes in soil type can lead to low Q_θ .
In this example, fingers of the Reakor association soils are interleaved with
the Delnorte association soils, causing rapid changes in pattern wavelength and
390 orientation, and consequently multiple energetic values of Θ and λ within the
260 m windows. Fig. 4c illustrates a region where the pattern orientation changes
rapidly, turning through approximately π radians within a single 260 m window.
Such rapid change inevitably leads to low Q_θ because there are multiple pattern
orientations located in a single window. There are also, however, regions near
395 the ridge crest where $Q_\theta \approx 1$ and the pattern is locally oriented perpendicular
to the slope. Fig. 4d is representative of the complex vegetation transitions that
occur near stream channels. Here, too, the pattern lies perpendicular to the local
hillslope orientation, and rather than curving into the streamline, remains broadly
aligned with the band orientation away from the stream.

400 (d) *Soil type effects*

While the vegetation patterns on the Delnorte soils have a unimodal
wavelength distribution, the Reakor soils exhibit a bimodal distribution (see
Fig. 3). The pattern associated with the second peak of λ on the Reakor soil
consists of bands of bare soil within a matrix of vegetation cover, inverting the

405 distribution in the remainder of the pattern. Visually, this ‘anti-stripe’ pattern is more disordered than the remainder of the pattern seen on the Reakor association soils. In the power spectra, these anti-stripe peaks contain less than half the power of the short wavelength, coherent peaks. Thus, on the Reakor association soils the pattern varies through space from short to long wavelength, ordered to disordered
410 patterns, and lower to higher biomass. Because increased biomass in drylands implies an increased access to water, we examine how λ varies as a function of the distance to the nearest stream (as a proxy for availability of water). The results are shown in Fig. 6. While patterns on the Delnorte soils did not show a distance-dependent λ ($r^2 = 0.08$ and $p = 0.4$), the patterns on Reakor soils show
415 a trend of increasing λ with decreasing distance to the nearest stream ($r^2 = 0.96$ and $p < 5 \times 10^{-7}$).

4. Discussion

The local Fourier metrics confirm Hypothesis (1) by showing that the wavelength and orientation of the vegetation patterns are typically coherent on scales of
420 600 – 800 m, but can change on scales of ≈ 20 m when the slope orientation changes over the same scale. We were unable to reproduce observed variation with a model even within regions of relatively uniform patterning, confirming Hypothesis (2) and further suggesting that exogenous factors rather than the pattern forming mechanisms drive the spatial variability in λ and Θ . In light
425 of these findings, and to address Hypothesis (3), our subsequent analysis focuses on the relationship between exogenous factors and the local pattern properties.

Our analysis indicates a hierarchy of controls on the morphology of the vegetation patterning: at a global scale the pattern morphology is determined by the slope orientation and the hillslope gradient, while the soil type imposes the
430 template for the pattern forming region. At smaller scales, complexity in the form of multiple local pattern orientations and deviations from the global trends are associated with ridges, streams, roads and changes in the soil type. Organization of the pattern characteristics on small scales arises due to a combination of soil type and topographic context: homogeneous, well defined patterns with a
435 unimodal λ on Delnorte soils, regardless of the topographic context. On Reakor association soils, the pattern λ increases in locations closer to streams, while the pattern simultaneously becomes more disordered and vegetation cover increases.

Several of these relationships support previous observations. The average hillslope gradient of 0.7% at the Fort Stockton site conforms to observations and
440 predictions of a minimum hillslope gradient being needed for band formation (Ursino & Contarini, 2006), and exceeds the minimum slope gradient observed in other settings (e.g. 0.25% in the Sudan (Deblauwe *et al.*, 2011)). In addition, the inverse relationship between pattern wavelength and the hillslope gradient (see Fig. 3) has been identified elsewhere (Valentin *et al.*, 1999; d’Herbès *et al.*, 2001;
445 Eddy *et al.*, 1999; Deblauwe *et al.*, 2011). However, the one model (Klausmeier,

1999) that has been used to study wavelength-gradient correlations predicts the *opposite* trend: steepness causes larger wavelengths (Sherratt, 2005; Ursino & Contarini, 2006). We explored this trend with a different model (Rietkerk *et al.*, 2002) and find that it also produces the opposite trend to that observed in natural
450 systems. While both models predict that multiple pattern wavelengths are stable for a given hillslope gradient (Sherratt & Lord, 2007; Thompson & Katul, 2009), the selection of particular longer or shorter wavelengths within that range is clearly at odds with observations.

The close correspondence between hillslope and pattern orientation at the
455 Fort Stockton site is a near-universal feature of vegetation patterning. The observed deviations generally arise due to local effects that disrupt the pattern, rapidly alter the direction of water flow, or change the strength and/or length-scales of the pattern forming feedbacks.

Pattern disruption is exemplified by the effects of roads (see Fig. 4a).
460 Roads disconnect upslope and downslope vegetation bands by preventing the redistribution of water. Rapid alteration of the direction of water flow occurs along ridges and stream channels. The pattern near these locations is less likely to have a unique orientation or wavelength than in the mid-slope areas, and is more likely to have a large $\Delta\Theta$. The prominent ridgeline shown in Fig. 4c is locally
465 surrounded by a region with $\Delta\Theta \approx \pi/2$ and $Q_\theta > 0.75$. This location provides an unambiguous example of a change in pattern orientation near no-flow boundary conditions, as predicted by McGrath *et al.* (2012). Other ridgelines are associated with large $\Delta\Theta$, but the low Q_θ in these locations makes the interpretation of the observed $\Delta\Theta$ ambiguous. Methods that identify a truly local metric of pattern
470 properties, instead of the quasi-local metric used here could both help to resolve these ambiguities, and to extend the analysis into patterned areas less than 260 m wide.

Stream channel locations are also associated with rapid, and sometimes discontinuous changes in pattern orientation. Like the ridge shown in Fig. 4c,
475 the stream channel shown in Fig. 4d is surrounded by a region where $\Delta\Theta \approx \pi/2$ and $Q_\theta > 0.75$, i.e. a unique pattern orientation that is perpendicular to the one expected from the slope orientation. There has been little exploration of the interaction of vegetation pattern with stream channels, presumably because the current paradigm of vegetation pattern models offer little reason to think
480 that such interactions would be important. Stream channels occur in locations where surface runoff rapidly flows away and therefore cannot affect vegetation upslope from the channel. However, we find evidence that the distance from a stream channel alters the pattern properties on the Reakor Association soil type. On these soils the pattern wavelength, vegetation cover and disorder increase
485 near the streams. These observations suggest that an additional mechanism could affect the patterning at this study site: for instance, the stream-channel boundary condition propagating back up into the hillslope.

We hypothesize that the ultimate cause of the changes in pattern morphology on the Reakor soils lies in the contrast in the soil depth between the Delnorte and

490 Reakor associations: from 23 cm to over 2 m. We are not the first to propose an
association between soil depth and the vegetation pattern structure. Depth to a
silcrete hardpan is associated with a transition between sharp patterns (shallow
hardpan) and diffuse patterns (deep or no hardpan) in Australia (Mabbutt &
Fanning, 1987; Tongway & Ludwig, 1990). Strikingly coherent vegetation bands
495 in Niger occur above a shallow ironstone hardpan (White, 1970). The broad,
diffuse banding near Fort Stockton studied by McDonald *et al.* (2008) occurs
on deep clays. McDonald *et al.* (2008) cited unpublished research claiming that
vegetated bands were associated with a local increase in the depth to the hardpan,
similar to previous observations of increased vegetation density on deep soils in
500 Australia (Mott & McComb, 1974).

Field evidence is needed to determine the exact mechanisms by which soil
depth and proximity to streams could lead to the changes we observed in pattern
morphology. Three scenarios illustrating potential mechanisms are shown in
Fig. 7 and could form the basis for future field studies. First, shallow soils
505 could promote lateral root extension by plants, exaggerating the effects of root
competition (Gilad *et al.*, 2004; Yizhaq *et al.*, 2005) (see Fig. 7ab). Studies of
Chihuahuan desert species confirm that there is intense root competition in the
zone above the petrocalcic horizon, where root growth is concentrated (Gibbens
& Lenz, 2001).

510 In the second scenario, we recognize that shallow surface soils have limited
water storage and saturate readily. For example, the Delnorte Association has as
little as 2 cm of water storage capacity in the soils above the impeding layer.
Unlike dry soils, which only generate runoff during very heavy rains, saturated
soils shed all rainfall as runoff. If soils did not saturate near plants this runoff
515 water could be trapped and infiltrate in these locations (see Fig. 7c). Plant roots
penetrate and thus may break up hardpans (Gibbens & Lenz, 2001). Root water
uptake is also a driver of hardpan formation (Duniway *et al.*, 2007), and hardpans
might thus form at greater depth beneath deep-rooted (woody) vegetation. Either
mechanism could prevent the surface soil from saturating near the vegetated
520 bands and allow it to store runoff.

The third scenario also relates to the potential for saturation to occur above
the hardpan, allowing subsurface saturated flow to occur (see Fig. 7c). The
changes in pattern properties with distance to the stream suggests that water
availability increases downslope: this requires subsurface storage, if not flow. A
525 relationship between the pattern formation and subsurface flow could explain the
local deviations of pattern orientation from slope orientation near the streamlines
since the surface orientation might not correspond to the local water table flow
direction.

All three scenarios would tend to strengthen the pattern forming feedbacks
530 on the shallow soils. They could be investigated using subsurface soil moisture
sensors to observe shallow soil saturation; water isotope tracers to determine
the water sources used by plants, observations of calcium ion concentrations in
runoff which would provide an indicator of water contact with the petrocalcic

535 horizon and root excavations to compare morphologies in sites with different depths to the impeding layer. These studies could be valuable to provide more information about the hydrological role of petrocalcic horizons, which have received relatively little attention given their ubiquity in desert environments (Duniway *et al.*, 2007).

5. Conclusion

540 Large scale analyses of variation in pattern morphology has provided broad confirmation of many theoretical predictions about vegetation patterning and its variation along climatic gradients (Deblauwe *et al.*, 2011), which are consistent with our observations at local scales. Our analysis shows that while pattern properties mostly vary on scales of 600 – 800 m, they can change much more
545 rapidly around boundaries in topography or soil characteristics. By analyzing the pattern on these fine scales, we identified deviations between hillslope and pattern orientation, soil-controlled changes in pattern wavelength, coherence and vegetation cover, and at least one likely example of the boundary condition effects predicted by McGrath *et al.* (2012). Two observations, echoed at
550 multiple other sites, are not well-explained by current theory: the observation of increasing pattern wavelength on steepness, and the soil controls on vegetation pattern length-scale and coherence.

The large timescale separation between individual storm events and the timescales on which desert vegetation distributions change means that an
555 ongoing dialogue between empirical and theoretical studies is critical for understanding the dynamics of these ecosystems. Local information about pattern qualities, when combined with high resolution information about the pattern substrate, is evidently a useful additional tool for analysis.

Despite the advances in understanding vegetation patterns in the past
560 ten years, theoretical models still require the use of effective parameters to describe feedbacks, soil-plant-water interactions and the resulting landscape fluxes. Linking theory and observation to make quantitative predictions, therefore, remains an outstanding challenge. Addressing this challenge requires improved observations of within-storm hydrologic processes and plant water
565 use: observations that ecohydrologists are increasingly equipped to make due to developments in distributed sensing systems and tracer technologies. Computational tools for assessing three-dimensional soil moisture dynamics, land-atmosphere interactions and vegetation spread are also improving. By coupling these tools with detailed field measurements, there is potential to
570 develop a detailed theoretical framework that can address the consequences of changing soil depth, root orientation, runoff generation mechanisms and subsurface flow processes on the overall dynamics and resilience of vegetation patterns.

6. Acknowledgements

575 SET and GP acknowledge support from NSF-EAR-1013339.

References

- Allen, J. & Rabiner, L. 1977 A unified approach to short-time Fourier analysis and synthesis. *Proceedings of the IEEE*, **65**(11), 1558 – 1564. (doi:10.1109/PROC.1977.10770)
- 580 Barbier, N., Couteron, P., Lefever, R., Deblauwe, V. & Lejeune, O. 2008 Spatial decoupling of facilitation and competition at the origin of gapped vegetation patterns. *Ecology*, **89**(6), 1521–1531. (doi:10.1890/07-0365.1)
- Borgogno, F., D’Odorico, P., Laio, F. & Ridolfi, L. 2009 Mathematical models of vegetation pattern formation in ecohydrology. *Reviews of Geophysics*,
585 **47**(RG1005). (doi:10.1029/2007RG000256)
- Bromley, J., Brouwer, J., Barker, A. P., Gaze, S. R. & Valentin, C. 1997 The role of surface water redistribution in an area of patterned vegetation in a semi-arid environment, south-west Niger. *Journal of Hydrology*, **198**(1-4), 1–29. (doi:10.1016/S0022-1694(96)03322-7)
- 590 Burton, G. J. & Moorhead, I. R. 1987 Color and spatial structure in natural scenes. *Applied Optics*, **26**(1), 157–170. (doi:10.1364/AO.26.000157)
- Caylor, K., Scanlon, T. & Rodriguez-Iturbe, I. 2004 Feasible optimality of vegetation patterns in river basins. *Geophysical Research Letters*, **31**(13), L13 502. (doi:10.1029/2004GL020260)
- 595 Couteron, P. & Lejeune, O. 2001 Periodic spotted patterns in semi-arid vegetation explained by a propagation-inhibition model. *Journal of Ecology*, **89**(4), 616–628.
- Cross, M. & Greenside, H. 2009 *Defects and fronts*, pp. 279–309. Cambridge University Press: Springer-Verlag, 1st edn.
- 600 Cross, M. C. & Hohenberg, P. C. 1993 Pattern formation out of equilibrium. *Reviews of Modern Physics*, **65**, 851–1112.
- Daniels, K. E., Brausch, O., Pesch, W. & Bodenschatz, E. 2008 Competition and bistability of ordered undulations and undulation chaos in inclined layer convection. *Journal of Fluid Mechanics*, **597**, 261–282. (doi:10.1017/S0022112007009615)
605

- Daubechies, I. 1990 The wavelet transform, time-frequency localization and signal analysis. *Information Theory, IEEE Transactions*, **36**(5), 961–1005. (doi:10.1109/18.57199)
- 610 Deblauwe, V., Couteron, P., Bogaert, J. & Barbier, N. 2012 Determinants and dynamics of banded vegetation pattern migration in arid climates. *Ecological Monographs*, **82**(1), 3–21. (doi:10.1890/11-0362.1)
- Deblauwe, V., Couteron, P., Lejeune, O., Bogaert, J. & Barbier, N. 2011 Environmental modulation of self-organized periodic vegetation patterns in Sudan. *Ecography*, **34**(6), 990–1001. (doi:10.1111/j.1600-0587.2010.06694.615 x)
- d’Herbès, J., Valentin, C., Tongway, D. & Leprun, J. 2001 Banded vegetation patterns and related structures. In *Banded vegetation patterning in arid and semiarid environments: ecological processes and consequences for management* (eds D. Tongway, C. Valentin & J. Seghier), no. 149 in 620 Ecological Studies, pp. 1–19. Springer.
- Duniway, M., Herrick, J. & Monger, H. 2007 The high water-holding capacity of petrocalcic horizons. *Soil Science Society of America Journal*, **71**(3), 812–819. (doi:10.2136/sssaj2006.0267)
- 625 Eckhaus, W. & Kuske, R. 1997 Pattern Formation in Systems with Slowly Varying Geometry. *SIAM Journal on Applied Mathematics*, **57**(1), 112–152. (doi:10.1137/S0036139994277531)
- Eddy, J., Humphreys, G., Hart, D., Mitchell, P. & Fanning, P. 1999 Vegetation arcs and litter dams: similarities and differences. *Catena*, **37**(1), 57–73. (doi:10.1016/S0341-8162(98)00055-1)
- 630 Egolf, D. 1998 Importance of local pattern properties in spiral defect chaos. *Physical Review Letters*, **80**(15), 3228–3231. (doi:10.1103/PhysRevLett.80.3228)
- Galle, S., Ehrmann, M. & Peugeot, C. 1999 Water balance in a banded vegetation pattern - a case study of tiger bush in western Niger. *Catena*, **37**(1-2), 197–635 216. (doi:10.1016/S0341-8162(98)90060-1)
- Gibbens, R. & Lenz, J. 2001 Root systems of some Chihuahuan Desert plants. *Journal of Arid Environments*, **49**(2), 221–263. (doi:10.1006/jare.2000.0784)
- 640 Gilad, E., von Hardenberg, J., Provenzale, A., Shachak, M. & Meron, E. 2004 Ecosystem engineers: From pattern formation to habitat creation. *Physical Review Letters*, **93**(9), 098 105. (doi:10.1103/PhysRevLett.93.098105)

- Greene, R. S. B. 1992 Soil physical properties of three geomorphic zones in a semiarid mulga woodland. *Australian Journal of Soil Research*, **30**(1), 55–69. (doi:10.1071/SR9920055)
- 645 Harman, C., Lohse, K. A., Troch, P. & Sivapalan, M. 2012 Co-evolution of resource islands and microtopography on semi-arid hillslopes. *Journal of Geophysical Research*, **In review**.
- Heutmaker, M., Fraenkel, P. & Gollub, J. 1985 Convection patterns: time evolution of the wave-vector field. *Physical Review Letters*, **54**(13). (doi:10.1103/PhysRevLett.54.1369)
- 650 HilleRisLambers, R., Rietkerk, M., van den Bosch, F., Prins, H. H. T. & de Kroon, H. 2001 Vegetation pattern formation in semi-arid grazing systems. *Ecology*, **82**(1), 50–61.
- Hu, Y., Ecke, R. & Ahlers, G. 1993 Convection near threshold for Prandtl numbers near 1. *Physical Review E*, **48**(6).
- 655 Kefi, S., Rietkerk, M., Alados, C. L., Pueyo, Y., Papanastasis, V. P., ElAich, A. & De Ruiter, P. C. 2007 Spatial vegetation patterns and imminent desertification in Mediterranean arid ecosystems. *Nature*, **449**(7159), 213–U5. (doi:10.1038/nature06111)
- Klausmeier, C. 1999 Regular and irregular patterns in semiarid vegetation. 660 *Science*, **284**(5421), 1826–1828. (doi:10.1126/science.284.5421.1826)
- Konings, A., Dekker, S., Rietkerk, M. & Katul, G. 2011 Drought sensitivity of patterned vegetation determined by rainfall-land surface feedbacks. *Journal of Geophysical Research*, **116**. (doi:10.1029/2011JG00174)
- 665 Larsen, L. & Harvey, J. 2011 Modeling of hydroecological feedbacks predicts distinct classes of wetland channel pattern and process that influence ecological function and restoration potential. *Geomorphology*, **126**(3–4), 279–296. (doi:10.1016/j.geomorph.2010.03.015)
- 670 Lefever, R., Barbier, N., Couteron, P. & Lejeune, O. 2009 Deeply gapped vegetation patterns: On crown/root allometry, criticality and desertification. *Journal of Theoretical Biology*, **261**(2), 194–209. (doi:10.1016/j.jtbi.2009.07.030)
- Lefever, R. & Lejeune, O. 1997 On the origin of tiger bush. *Bulletin of Mathematical Biology*, **59**, 263–294. (doi:10.1007/BF02462004)
- 675 Lindner, B. 2004 Effects of noise in excitable systems. *Physics Reports*, **392**(6), 321–424. (doi:10.1016/j.physrep.2003.10.015)

- Lowe, M., Gollub, J. & Lubensky, T. 1983 Commensurate and incommensurate structures in a nonequilibrium system. *Physical Review Letters*, **51**(9), 786–789. (doi:10.1103/PhysRevLett.51.786)
- Mabbutt, J. & Fanning, P. 1987 Vegetation banding in arid Western Australia. *Journal of Arid Environments*, **12**(1), 41–59. 680
- Macfadyen, W. 1950 Vegetation patterns in the semi-desert plains of British Somaliland. *Geographical Journal*, pp. 199–211.
- McDonald, A., Kinucan, R. & Loomis, L. 2008 Ecohydrological interactions within banded vegetation in the northeastern Chihuahuan Desert, USA. *Ecohydrology*, **2**(1). (doi:10.1002/eco.40) 685
- McGrath, G., Paik, K. & Hinz, C. 2012 Microtopography alters self-organized vegetation patterns in water-limited ecosystems. *Journal of Geophysical Research*, **117**(G03021). (doi:10.1029/2011JG001870)
- Meron, E., Gilad, E., von Hardenberg, J., Shachak, M. & Zarmi, Y. 2004 Vegetation patterns along a rainfall gradient. *Chaos Solitons & Fractals*, **19**(2), 367–376. (doi:10.1016/S0960-0779(03)00049-3) 690
- Mott, J. & McComb, A. 1974 Patterns in annual vegetation and soil microrelief in arid region of Western Australia. *Journal of Ecology*, **62**(1), 115–126.
- National Agricultural Imaging Program 2010 Pecos county. <http://gis.apfo.usda.gov/arccgis/services>. 695
- National Climatic Data Center 2010 Fort Stockton climate annual summary. <http://www.ncdc.noaa.gov/cdo-web/datasets/ANNUAL/locations/ZIP:79735/detail>.
- Oimoen, M. 2000 An effective filter for removal of production artifacts in U.S. Geological Survey 7.5 minute digital elevation models. Tech. rep., USGS EROS Data Center, Sioux Falls, South Dakota. 700
- Pinnegar, C. & Mansinha, L. 2004 Time-local Fourier analysis with a scalable, phase-modulated analyzing function: The s-transform with a complex window. *Signal Processing*, **84**(7), 1167 – 1176. (doi:10.1016/j.sigpro.2004.03.015) 705
- Pringle, R. M., Doak, D. F., Brody, A. K., Jocqué, R. & Palmer, T. M. 2010 Spatial pattern enhances ecosystem functioning in an african savanna. *PLoS biology*, **8**(5), e1000377. (doi:10.1371/journal.pbio.1000377)

- 710 Puigdefábregas, J. 2005 The role of vegetation patterns in structuring runoff and
sediment fluxes in drylands. *Earth Surface, Processes and Landforms*, **30**,
133–147. (doi:10.1002/esp.1181)
- Ravi, S., D’Odorico, P., Wang, L. & Collins, S. 2008 Form and function of grass
ring patterns in arid grasslands: The role of abiotic controls. *Oecologia*, **158**,
545–555. (doi:10.1007/s00442-008-1164-1)
- 715 Richards, J. 1999 *Supervised classification techniques: Thresholds*, pp. 185–189.
Berlin: Springer-Verlag, 2nd edn.
- Rietkerk, M., Boerlijst, M. C., van Langevelde, F., HilleRisLambers, R., van de
Koppel, J., Kumar, L., Prins, H. H. T. & de Roos, A. M. 2002 Self-organization
of vegetation in arid ecosystems. *American Naturalist*, **160**(4), 524–530. (doi:
720 10.1086/342078)
- Rietkerk, M., Dekker, S., de Ruiter, P. & van de Koppel, J. 2004a Self-organized
patchiness and catastrophic shifts in ecosystems. *Science*, **305**(5692), 1926–
1929.
- Rietkerk, M., Dekker, S., Wassen, M., Verkroost, A. & Bierkens, M. 2004b A
725 putative mechanism for bog patterning. *The American Naturalist*, **163**(5),
699–708.
- Scanlon, T. M., Caylor, K. K., Levin, S. A. & Rodriguez-Iturbe, I. 2007 Positive
feedbacks promote power-law clustering of Kalahari vegetation. *Nature*,
449(7159), 209–212. (doi:10.1038/nature06060)
- 730 Scheffer, M., Bascompte, J., Brock, W., Brovkin, V., Carpenter, S., Dakos, V.,
Held, H., Van Nes, E., Rietkerk, M. *et al.* 2009 Early-warning signals for
critical transitions. *Nature*, **461**(7260), 53–59.
- Schlesinger, W. H., Reynolds, J., Cunningham, G., Huenneke, L., Jarrell,
W., Virginia, R. & Whitford, W. 1990 Biological feedbacks in global
735 desertification. *Science*, **147**, 1043–1048.
- Scholes, R. J. & Archer, S. R. 1997 Tree-grass interactions in savannas. *Annual
Review of Ecology and Systematics*, **28**, 517–544.
- Seghieri, J., Galle, S., Rajot, J. L. & Ehrmann, M. 1997 Relationships between
soil moisture and growth of herbaceous plants in a natural vegetation mosaic
740 in Niger. *Journal of Arid Environments*, **36**(1), 87–102.
- Sherratt, J. 2005 An analysis of vegetation stripe formation in semi-arid
landscapes. *Journal of Mathematical Biology*, **51**(2), 183–197. (doi:10.1016/
j.tpb.2006.07.009)

- 745 Sherratt, J. & Lord, G. 2007 Nonlinear dynamics and pattern bifurcations
in a model for vegetation stripes in semi-arid environments. *Theoretical
Population Biology*, **71**(1), 1–11. (doi:10.1016/j.tpb.2006.07.009)
- Thiéry, J., D’Herbès, J. & Valentin, C. 1995 A model simulating the genesis
of banded vegetation patterns in Niger. *Journal of Ecology*, **83**(3), 497–507.
(doi:10.2307/2261602)
- 750 Thompson, S. & Daniels, K. 2010 A porous convection model for grass patterns.
The American Naturalist, **175**(1), E10–E15. (doi:10.1086/648603)
- Thompson, S. E., Harman, C. J., Troch, P. A., Brooks, P. D. & Sivapalan, M.
2011a Scaling of ecohydrologically mediated water balance partitioning: A
synthesis framework for catchment ecohydrology. *Water Resources Research*,
755 **47**(W00J03). (doi:10.1029/2010WR009998)
- Thompson, S. E., Katul, G., Konings, A. & Ridolfi, L. 2011b Unsteady overland
flow on flat surfaces induced by spatial permeability contrasts. *Advances in
Water Resources*, **34**, 1049–1058. (doi:10.1016/j.advwatres.2011.05.012)
- 760 Thompson, S. E. & Katul, G. G. 2009 Secondary seed dispersal and its role
in landscape organization. *Geophysical Research Letters*, **36**(L02402). (doi:
10.1029/2008GL036044)
- Thompson, S. E., Katul, G. G. & MacMahon, S. 2008 Role of biomass spread
in vegetation pattern formation within arid ecosystems. *Water Resources
Research*, **44**(E10421). (doi:10.1029/2008WR006916)
- 765 Tolhurst, D. J., Tadmor, Y. & Chao, T. 1992 Amplitude spectra of natural images.
Ophthalmic and Physiological Optics, **12**(2), 229–232. (doi:10.1111/j.1475-
1313.1992.tb00296.x)
- Tongway, D. J. & Ludwig, J. A. 1990 Vegetation and soil patterning in semi-
arid mulga lands of Eastern Australia. *Australian Journal of Ecology*, **15**(1),
770 23–34. (doi:10.1111/j.1442-9993.1990.tb01017.x)
- Ursino, N. & Contarini, S. 2006 Stability of banded vegetation patterns under
seasonal rainfall and limited soil moisture storage capacity. *Advances in Water
Resources*, **29**, 1556–1564. (doi:10.1016/j.advwatres.2005.11.006)
- 775 Valentin, C., d’Herbes, J. & Poesen, J. 1999 Soil and water components of
banded vegetation patterns. *Catena*, **37**(1-2), 1 – 24. (doi:10.1016/S0341-
8162(99)00053-3)
- Van de Koppel, J., Gascoigne, J., Theraulaz, G., Rietkerk, M., W.M., M. &
Herman, P. 2008 Experimental evidence for spatial self-organization and
its emergent effects in mussel beds. *Science*, **322**(5902), 739–742. (doi:
780 10.1126/science.1163952)

- von Hardenberg, J., Kletter, A. Y., Yizhaq, H., Nathan, J. & Meron, E. 2010
Periodic versus scale-free patterns in dryland vegetation. *Proceedings of the
Royal Society B-Biological Sciences*, **277**(1688), 1771–1776.
- 785 White, L. 1970 *Brousse tigrée* patterns in southern Niger. *The Journal of
Ecology*, **58**(2), 549–553.
- Worrall, G. 1960 Tree patterns in the Sudan. *Journal of Soil Science*, **11**(1),
63–67.
- 790 Yizhaq, H., Gilad, E. & Meron, E. 2005 Banded vegetation: Biological
productivity and resilience. *Physica A-Statistical Mechanics and Its
Applications*, **356**(1), 139–144.

7. Tables

Table 1. Pattern characteristics of natural patterning across the full pattern extent.

	Mean	Std. Dev.	Corr. Length (m)
Pattern wavelength, $\bar{\lambda}$ (m)	63	13.8	800
Mean pattern orientation, $\bar{\Theta}$ (rads)	1.4	0.76	600
Hillslope orientation (rad)	1.2	0.75	1400
Hillslope gradient	0.007	0.002	1900

Table 2. Soil properties for the Delnorte and Reakor Association Soils. Note that the soil textural percentages do not sum to 100 because gravel and organic content have not been reported.

	Reakor	Delnorte
Soil depth (cm)	200	23
Hydraulic conductivity (K_{sat} , $\mu\text{m s}^{-1}$)	2.1	59.2
Clay content (%)	31.5	8.7
Sand content (%)	6.8	42.8
Silt content (%)	61.7	21.1

Table 3. Pattern characteristics comparing analysis of natural and simulated data for a $500 \times 800 \text{ m}^2$ region. The simulated data comes from a modified Rietkirk model calibrated to match the mean pattern properties of the natural data.

	Mean	Std. Dev.	Corr. Length (m)
Natural pattern wavelength $\bar{\lambda}$ (m)	53	4.1	350
Model pattern wavelength $\bar{\lambda}$ (m)	54	1.7	360
Natural pattern orientation $\bar{\Theta}$ (rad)	1.7	0.39	420
Model pattern orientation $\bar{\Theta}$ (rad)	1.6	0.07	390
Hillslope orientation (rad)	1.7	0.5	120

8. Figures

h

Figure 1. (a) Binary image of the Fort Stockton region, covering an $\approx 188 \text{ km}^2$ area. Vegetation is shown as black and bare soil is shown as white. (b) Detail of size $260 \times 260 \text{ m}^2$, showing the original detailed image. (c) Binary image detail.

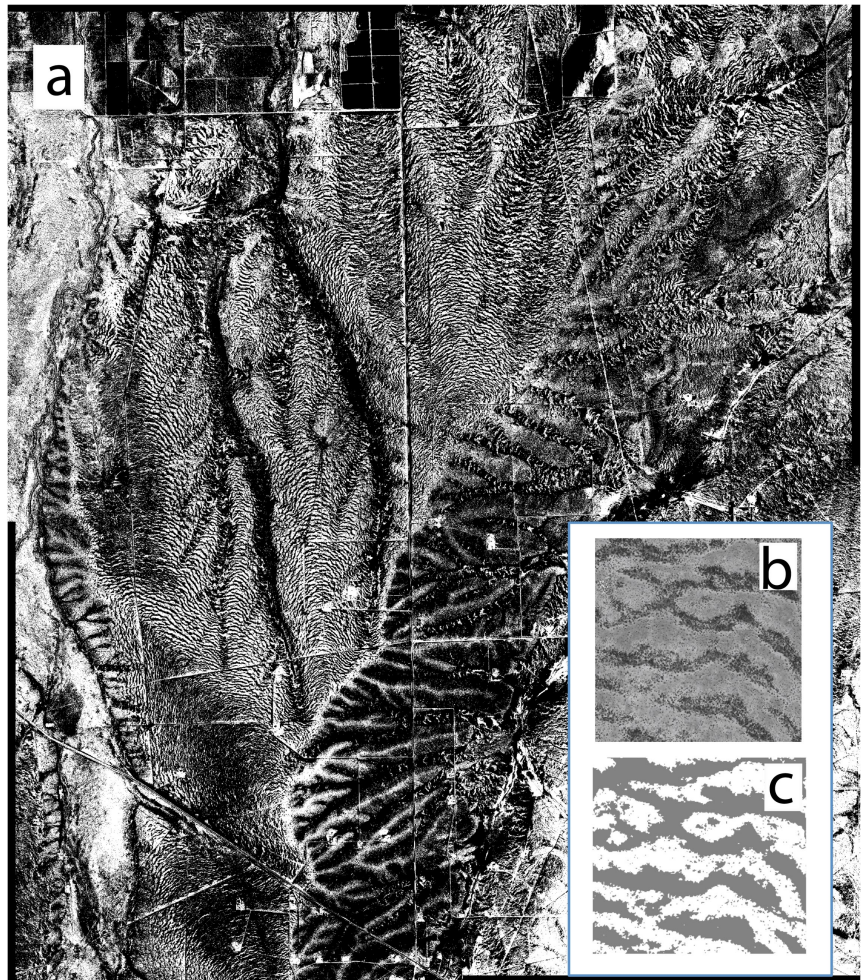


Figure 2. Maps of (a) local wavelength $\lambda(x,y)$, with color scale indicating wavelength in meters and (b) local orientation $\Theta(x,y)$, with color scale indicating orientation in radians. Areas in white do not contain patterns as recognized by the Fourier windowing method.

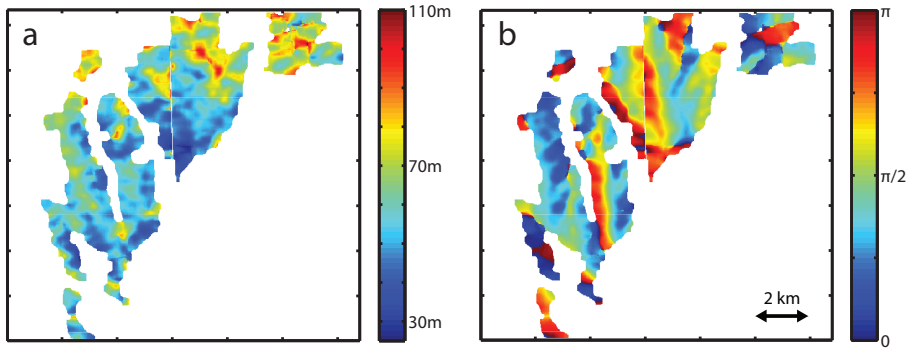


Figure 3. (a) Frequency distribution of $\Delta\Theta$, the deviation between the local pattern orientation and the local topographic orientation. The slope orientations deviate by less than $\pi/8$ for 80% of the image. (b) Comparison of the local pattern wavelength λ to the local topographic slope. Data were collected into 10 bins of equal size (≈ 11000 data points per bin). The box and whisker plots indicate the median (central lines); the 25th and 75th quartiles (box limits) within the bin. The whiskers extend two inter-quartile ranges from the median. The thick red line indicates a linear fit to the medians. (c) PDF of the pattern wavelengths associated with the two major soil classes, indicating the bimodality in λ on Reakor association soils.

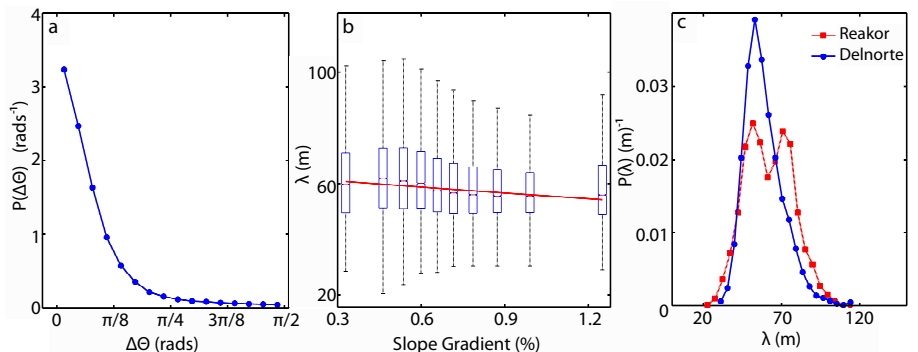


Figure 4. Spatial distribution of the uniqueness metric Q_{Θ} for the pattern orientation, and magnified cases illustrating different examples of non-uniqueness in the pattern orientation. Panel (a) indicates non-uniqueness in orientation associated with a road, which adds north-south oriented structure to the local NE-SW oriented banding due to upslope ponding of runoff. Panel (b) indicates a region of changing pattern orientation and wavelength associated with the interleaving of two contrasting soil types. Panel (c) illustrates the short length-scales on which the pattern can change orientation as it bends around a sharp ridge (location indicated in blue). A proportion of the region where $\Delta\Theta \approx \pi/4$, as indicated by the different director arrows, has $Q_{\Theta} > 0.75$. Panel (d) indicates the deviation between pattern and slope orientation around a stream channel (estimated location shown in blue); again there are regions where $\Delta\Theta \approx \pi/2$ and $Q_{\Theta} > 0.75$.

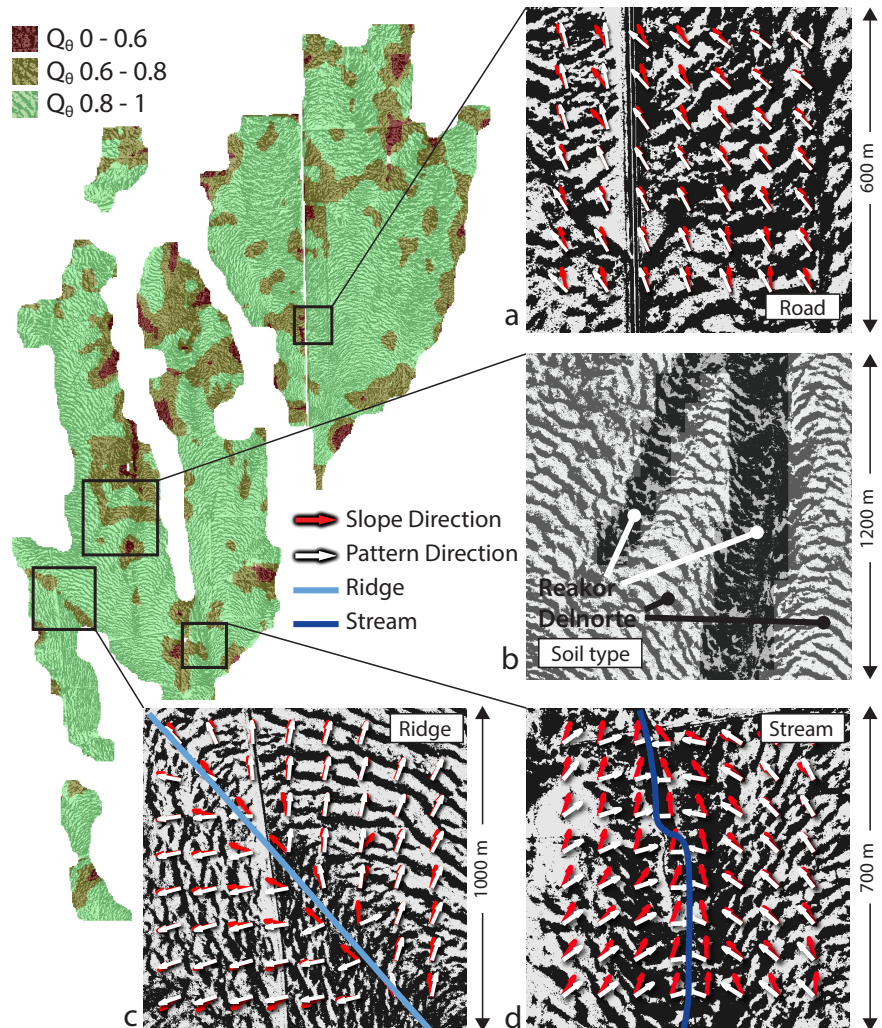


Figure 5. Relative increase in frequency of (a,b) non-unique pattern orientations and (c) wavelengths, for windows within 250 m of local elevation minima (streams), maxima (ridges), roads, and pattern boundaries. All frequencies are measured relative to the frequency in the remainder of the pattern. Non-unique orientations, for example, occurred 50-60% more often near streamlines and ridges than in the bulk of the pattern.

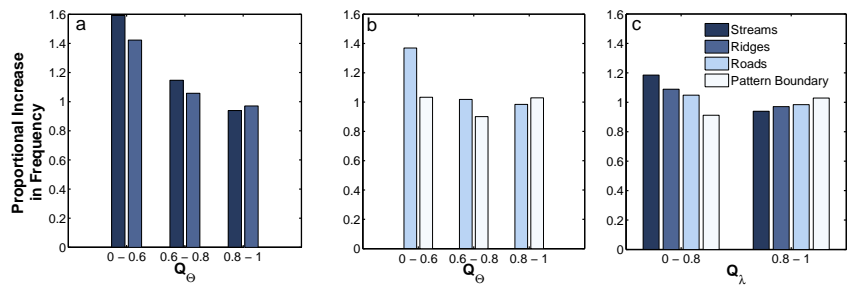


Figure 6. Distribution of the soils within the pattern forming areas with respect to landscape position, referenced to the nearest stream channel or local elevation minimum for (a) Reakor and (b) Delnorte Association soils. Although both soil types occur across the range of landscape positions, the Reakor association soils are more strongly associated with riparian areas. Distribution of pattern wavelengths on the Reakor Association (c) and Delnorte Association (d) soils with respect to the nearest stream, again based on equally-sized bins of the dataset. There is a strong ($r^2 = 0.96$) and significant ($p < 5 \times 10^{-7}$) decline in the wavelength on Reakor soils when moving from the riparian areas to the uplands. There is no correlation between landscape position and pattern properties on the Delnorte association ($r^2 = 0.08$ and $p = 0.4$).

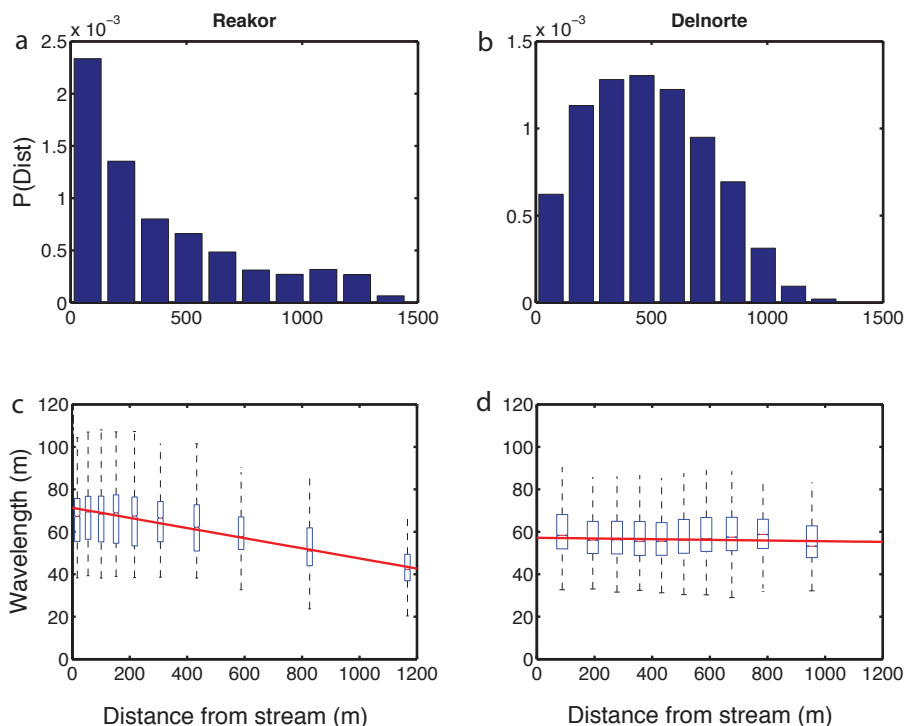


Figure 7. Schematic illustration of possible effects of a shallow impeding layer on pattern formation mechanisms. (a) In the absence of an impeding layer, plants develop deep root systems to exploit water from across the whole soil profile (b) A shallow impeding layer restricts the vertical growth of roots, confining them to the surface soils, and promoting root competition laterally. (c) The shallow impeding layer also creates the potential for complex subsurface hydrology. Saturation of soils above the impeding layer may promote saturation excess runoff. Gradients - due to changes in the depth of the impeding layer, or in water potential across the impeding layer - can also induce saturated porous media flow. Provided that surface soils near plants can freely drain, the altered hydrology may exaggerate the positive feedback between plants and water.

